GMR
The Original

ULTRASOUND-ASSISTED GREEN FABRICATION OF CUO NANOPARTICLES INTEGRATED WITH STARCH/PVA NANOFIBROUS SCAFFOLDS FOR WOUND REPAIR APPLICATIONS

Pooja Yagavel[1], Anoosh Golla[2], Abyramy Balasundaram[3], Alagendran Subbarayalu[4], Kaliyamoorthy Dass[5*]

[1]Saveetha Medical College & Hospital (SMCH), Saveetha Institute of Medical and Technical Sciences (SIMATS), Thandalam, Chennai, Tamil Nadu 602105, India. Email: poojay@gmail.com
[2]Department of Neurology, Saveetha Medical College and Hospital, Saveetha Institute of Medical And Technical Sciences (SIMATS), Thandalam, Chennai-602105, Tamil Nadu, India. Email: anushyadav2025@gmail.com
[3]Department of Dermatology, Saveetha Medical College and Hospital, Saveetha Institute of Medical And Technical Sciences (SIMATS), Thandalam, Chennai-602105, Tamil Nadu, India. Email: b.abyramy@gmail.com; ORCID: https://orcid.org/0000-0002-0534-6225
[4]Saveetha College of Nursing (SCON), Saveetha Institute of Medical and Technical Sciences (SIMATS), Chennai – 602105, Tamil Nadu, India. Email: alagendrans.scon@saveetha.com; ORCID: https://orcid.org/0009-0009-0749-7180
[5*]Natural Product and Vector Control Research Lab, Department of Pharmacology, Saveetha Medical College and Hospital, Saveetha Institute of Medical And Technical Sciences (SIMATS), Thandalam, Chennai-602105, Tamil Nadu, India. Email: dass.smc@saveetha.com; ORCID: https://orcid.org/0000-0002-4564-3275

ABSTRACT

This work presents a sustainable strategy for designing bioactive nanofibrous materials aimed at improving skin regeneration. Copper oxide nanoparticles were generated through an ultrasound-assisted process utilizing biomolecules derived from the marine alga *Turbinaria ornata*, eliminating the need for hazardous chemical reagents. These nanostructures were subsequently embedded within electrospun fibers composed of starch and polyvinyl alcohol to construct a hybrid scaffold with enhanced functional properties. Comprehensive physicochemical evaluation demonstrated the successful formation of CuO nanoparticles and their uniform incorporation within the fibrous matrix. Spectroscopic and diffraction analyses confirmed the structural integrity of both the nanoparticles and the polymer network, while microscopic observations revealed a continuous, porous architecture favorable for biological interactions. Thermal studies further indicated improved stability of the composite system following nanoparticle incorporation. The biological performance of the developed material was assessed using a keratinocyte-based scratch model. A marked improvement in cellular migration was observed in a concentration-dependent manner, with the composite scaffold exhibiting superior regenerative performance compared to individual components. At higher concentrations, the system facilitated near-complete wound closure, highlighting its effectiveness in promoting tissue repair. Overall, the findings demonstrate that integrating marine-derived bioactive agents with metal oxide nanostructures within an electrospun platform offers a promising route for developing advanced wound dressing materials with enhanced therapeutic functionality.

KEYWORDS: *Turbinaria ornata*, Ultrasound extraction, Green synthesis, CuO nanoparticles, Polymeric nanoscaffolds, Wound healing.

INTRODUCTION

The repair of injured skin is a highly coordinated and dynamic biological process that involves a series of overlapping phases, including hemostasis, inflammation, proliferation, and tissue remodeling [1]. This process can be significantly disrupted by various internal and external factors such as microbial invasion, excessive oxidative stress, and impaired cellular signaling. In particular, chronic wounds commonly associated with conditions such as diabetes, vascular insufficiency, and aging pose a serious clinical challenge due to their prolonged healing duration and increased risk of infection [2]. These wounds often fail to progress through the normal stages of healing, resulting in persistent inflammation and delayed tissue regeneration. Although conventional wound dressings, such as gauze and cotton-based materials, provide basic protection, they are generally passive in nature and lack the ability to actively support biological repair mechanisms or regulate the wound microenvironment [3, 4].

In response to these limitations, recent research has increasingly focused on the development of advanced biomaterials that can more effectively promote tissue regeneration. A key strategy in this area involves designing materials that replicate the architecture and function of the natural extracellular matrix (ECM), which plays a critical role in guiding cell behavior [5]. Electrospinning has emerged as a powerful technique for fabricating nanofibrous scaffolds that closely resemble the fibrous structure of the ECM [6]. These materials are characterized by high surface area, interconnected porosity, and tunable properties, all of which contribute to enhanced cell adhesion, proliferation, and nutrient transport [7]. Among the various polymers used for electrospinning, polyvinyl alcohol (PVA) is particularly attractive due to its

excellent mechanical strength, water solubility, and ease of processing [8]. However, PVA alone does not possess sufficient biological activity, which limits its effectiveness in regenerative applications [9].

To address this limitation, natural polymers are often incorporated into synthetic systems to improve their biological performance [10]. Starch, a naturally abundant polysaccharide, offers several advantages including biocompatibility, biodegradability, and structural similarity to native biological tissues [11]. When combined with PVA, starch can enhance the overall functionality of the scaffold by improving its hydrophilicity and promoting cell material interactions [12]. In addition to polymer blending, the incorporation of nanoscale components has gained considerable attention as a means of introducing new functionalities into biomaterials. Metal oxide nanoparticles, particularly copper oxide (CuO), have been extensively studied for their unique physicochemical and biological properties [13]. These nanoparticles exhibit strong antimicrobial activity, catalytic behavior, and the ability to influence cellular processes such as angiogenesis and collagen synthesis, all of which are essential for effective wound healing [14].

An important advancement in nanoparticle synthesis is the shift toward environmentally sustainable methods. Traditional chemical synthesis routes often involve hazardous reagents and generate toxic byproducts, raising concerns regarding environmental safety and biocompatibility [15]. In contrast, green synthesis approaches utilize natural biological systems as both reducing and stabilizing agents, enabling the formation of nanoparticles under mild and eco-friendly conditions. Marine macroalgae, in particular, are rich in bioactive compounds such as polyphenols, flavonoids, and polysaccharides, which can facilitate nanoparticle formation while simultaneously imparting biological functionality [16]. Turbinaria ornata, a brown seaweed widely distributed in coastal regions, has attracted attention due to its antioxidant, antimicrobial, and anti-inflammatory properties, making it a promising candidate for biomedical applications [17].

Integrating green-synthesized nanoparticles with electrospun polymeric scaffolds represents a promising strategy for developing multifunctional wound dressing materials. Such hybrid systems combine the structural advantages of nanofibrous matrices with the therapeutic properties of bioactive nanoparticles, resulting in materials that can actively participate in the healing process [18, 19]. In this study, a novel composite scaffold was developed by incorporating CuO nanoparticles synthesized from T. ornata extract into a starch/PVA electrospun matrix. The work aims to systematically evaluate the structural, physicochemical, and biological properties of the resulting material. Furthermore, its ability to enhance cellular migration and promote wound closure is assessed using an in vitro model, providing insight into its potential as an advanced platform for wound healing applications.

2. Materials and methods

2.1. Collection and preparation of marine biomass

Specimens of the brown macroalga Turbinaria ornata were collected from coastal waters near Rameswaram, Tamil Nadu, India. The harvested material was thoroughly cleaned to remove extraneous matter through sequential rinsing with tap water followed by distilled water to eliminate residual salts and impurities. The cleaned biomass was cut into smaller segments and dried under ambient conditions until complete dehydration was achieved. The dried samples were subsequently ground into a fine powder and stored in airtight containers for further experimental use.

2.2. Ultrasonic-assisted extraction

To obtain bioactive compounds, the dried algal powder was first introduced into purified water to create an aqueous extraction system, ensuring adequate contact between the solvent and plant matrix. The mixture was then exposed to ultrasonic energy under controlled temperature conditions (60°C) for a duration of 45 minutes. This acoustic treatment facilitates the disruption of cell walls through cavitation effects, thereby promoting the efficient release of intracellular metabolites into the surrounding medium. After completion of the extraction process, the suspension was allowed to settle briefly and subsequently clarified by passing it through a filtration medium to separate residual solid particles from the liquid phase. The collected extract, containing dissolved bioactive constituents, was preserved at a low temperature (10°C) to maintain its chemical stability for immediate experimental use. For long-term storage and further applications requiring a solid form, a portion of the liquid extract was subjected to lyophilization. This process removes water under reduced pressure and low temperature, yielding a dry, stable powder while preserving the integrity of thermolabile compounds. The resulting extract was then stored under appropriate conditions until further utilization [20, 21].

2.3. Green synthesis of CuO nanoparticles

Copper oxide nanostructures were generated using a green synthesis strategy in which bioactive molecules derived from the algal extract acted as both reducing and stabilizing agents. For this purpose, an aqueous copper salt solution was prepared and subsequently mixed with the previously obtained algal extract in a defined proportion to initiate the reaction. The presence of phytochemicals within the extract enables the transformation of copper ions into nanoscale copper oxide through a biologically driven reduction process. The reaction system was maintained under controlled thermal conditions at 60°C while being continuously agitated to ensure uniform mixing and consistent nucleation throughout the solution. Sustained stirring promotes homogeneous growth of nanostructures and prevents localized aggregation during the formation stage. Over the course of the reaction period, a distinct shift in solution color from blue to a bluish-green hue served as a visual indicator of nanoparticle generation, reflecting changes in the electronic structure associated with nanoscale copper oxide formation. Following completion of the synthesis, the reaction mixture was subjected to high-speed centrifugation to isolate the formed nanostructures from the surrounding liquid medium. The collected particles were then purified through multiple washing cycles using double-distilled water in order to eliminate any unreacted precursors and residual organic components. Finally, the purified material was subjected to freeze-drying for an extended

period, yielding a dry nanoparticulate powder with improved stability and suitability for subsequent characterization and application [22].

2.4. Fabrication of CuO-loaded starch/PVA nanoscaffolds

A polymeric base solution was first formulated by dissolving fully hydrolyzed polyvinyl alcohol in water under controlled heating conditions, accompanied by continuous stirring to ensure complete solubilization and uniform consistency. Once a clear and stable solution was obtained, starch and the previously synthesized copper oxide nanostructures were introduced into the system. The mixture was maintained at an elevated temperature of 50°C and subjected to prolonged stirring to facilitate uniform distribution of both the natural polymer and the inorganic nanomaterial within the polymer matrix. This step is essential to achieve a well-dispersed composite solution, which directly influences the structural integrity of the final fibers. The prepared blend was subsequently loaded into a syringe equipped with a fine-gauge metallic needle and processed through an electrospinning setup to generate nanofibrous structures. A high-voltage electric field was applied to induce the formation of a continuous polymer jet, which underwent stretching and solvent evaporation during its travel toward the collector. Key operational parameters, including the applied voltage, flow rate of the polymer solution, and the distance between the needle tip and collector, were carefully regulated to obtain uniform fibers with minimal defects. The electrospinning process was allowed to proceed for several hours under ambient environmental conditions, leading to the gradual deposition of interconnected nanofibers on the collector surface. The resulting material formed a porous, nonwoven mat with nanoscale fiber dimensions, suitable for applications requiring high surface area and structural mimicry of biological tissues [23-25].

2.5. Physicochemical characterization

The optical response of the prepared samples was analyzed using UV–visible spectroscopic techniques to monitor changes associated with nanoparticle formation and composite development. Measurements were performed across a broad spectral window spanning 200 to 800 nm in order to capture characteristic absorption features of both organic constituents and inorganic nanostructures. Prior to analysis, deionized water was used as a baseline reference to ensure accurate normalization of the recorded spectra. The resulting absorption profiles were subsequently interpreted to identify shifts in electronic transitions and spectral signatures indicative of successful nanoparticle generation and their interaction within the composite system [26].

Infrared spectroscopic analysis was carried out using an attenuated total reflectance (ATR) configuration to investigate the chemical functionalities present in the samples. The measurements were conducted across a broad wavenumber interval extending from 4000 to 400 cm^{-1}, allowing comprehensive detection of both high- and low-frequency vibrational modes. For each sample, multiple scans were accumulated to enhance signal quality and reproducibility, with the instrument operating at a spectral resolution sufficient to clearly resolve characteristic absorption bands. The acquired spectra were systematically interpreted to assign vibrational signatures corresponding to specific chemical groups, thereby enabling confirmation of the material composition and the presence of interactions between organic constituents and inorganic nanostructures within the system [27].

The structural organization and phase characteristics of both the copper oxide nanostructures and the corresponding composite scaffolds were examined through X-ray diffraction analysis. Measurements were carried out using a Bruker D8 Advance diffractometer equipped with CuKα radiation (λ = 1.5406 Å), operating under conditions of 40 kV and 40 mA. Diffraction data were acquired across a wide angular range (2θ = 5°–90°) to ensure comprehensive detection of crystalline reflections. The resulting diffraction profiles were utilized to evaluate the degree of crystallinity, identify characteristic lattice planes, and verify the successful formation of copper oxide phases as well as their incorporation within the polymeric matrix [28].

The surface architecture of the electrospun fibrous matrices, along with the spatial arrangement of embedded nanoparticles, was investigated using scanning electron microscopy. Prior to imaging, each specimen was coated with a fine conductive layer of gold to minimize charging effects and enhance image clarity. This preparation step enabled high-resolution visualization of fiber morphology, including surface texture, continuity, and the distribution pattern of nanoscale inclusions within the scaffold network [29].

The thermal behavior and degradation profile of the fabricated composite scaffolds were assessed through thermogravimetric analysis. A small quantity of each sample (approximately 5 mg) was subjected to a controlled heating program, beginning at ambient temperature and progressing up to 550°C at a constant rate of 15°C per minute. The analysis was conducted under an inert nitrogen environment to prevent oxidative interference during thermal decomposition. The resulting mass loss patterns were carefully examined to determine the stability of the material, identify distinct degradation stages, and evaluate the influence of incorporated nanostructures on the thermal resistance of the polymer matrix [30].

The size characteristics and dispersion behavior of the synthesized copper oxide nanostructures were investigated using dynamic light scattering in conjunction with surface charge analysis. Measurements were performed with a Malvern Zetasizer Ultra to obtain the hydrodynamic diameter distribution of the particles in suspension. In parallel, zeta potential values were recorded to assess the electrostatic stability of the colloidal system. Together, these analyses provide insight into particle aggregation tendencies and suspension stability, which are critical parameters influencing the performance of nanostructures in biological and material applications [31]. All related data are publicly accessible on the Mendeley Data repository (DOI: 10.17632/tgxw2g4stx.1).

2.6. In Vitro wound healing assay

The regenerative performance of the developed materials was investigated using an in vitro wound healing model based on HaCaT keratinocyte cells. Cells were initially cultured in 12-well plates at a density of 2×10^5 cells per well using Dulbecco's Modified Eagle Medium (DMEM) supplemented with 10% fetal bovine serum and 1% penicillin–streptomycin. The cultures were maintained under standard conditions until a continuous and confluent monolayer was established. To simulate a wound environment, a linear gap was introduced across the cell layer using a sterile pipette tip, thereby creating a reproducible cell-free region. Following scratch formation, non-adherent and detached cells were gently removed by rinsing with phosphate-buffered saline (PBS). The remaining adherent cells were then exposed to different treatment conditions, including algal extract, copper oxide nanostructures, and nanofibrous scaffold formulations at concentrations ranging from 6.25 to 100 µg/mL, all prepared in serum-free medium. Cells maintained without any treatment served as the control group. The progression of wound closure was monitored at specific time intervals (0, 24, and 48 hours) using phase-contrast microscopy to capture changes in the cell-free region. Quantitative analysis of cell migration was performed using ImageJ software by measuring the reduction in wound area over time. This approach enabled a comparative assessment of the ability of each treatment to promote cellular movement and facilitate wound closure [32].

2.7. Statistical analysis

All experimental procedures were conducted in three independent replicates to ensure reproducibility, and the obtained data are expressed as mean values accompanied by standard deviation. Statistical evaluations were performed using SPSS software (version 25.0) in combination with GraphPad Prism (version 9.0) for data analysis and visualization. Comparative analysis among different experimental groups was carried out using one-way analysis of variance (ANOVA), followed by appropriate post hoc multiple comparison tests, including Tukey's and Dunnett's methods, to identify statistically meaningful differences. A threshold value of $p < 0.05$ was adopted to determine statistical significance. To further explore potential relationships between variables, Pearson correlation analysis was applied. Additionally, the distribution characteristics of the datasets were assessed using the Shapiro–Wilk normality test to ensure the validity of parametric statistical approaches [33].

3. RESULTS

3.1. UV-visible spectroscopy

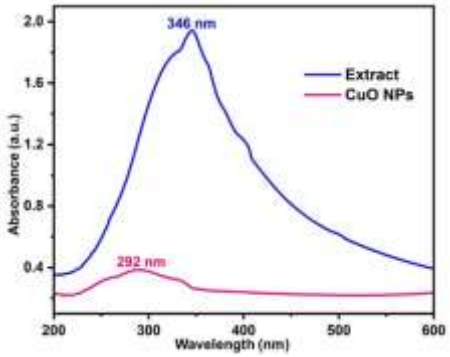

Figure 1. Optical absorption behavior of Turbinaria ornata extract compared with biosynthesized copper oxide nanostructures.

UV–visible spectral analysis (Figure 1) revealed distinct optical signatures for the T. ornata extract and the synthesized CuO nanoparticles. The algal extract displayed a broad absorption profile within the 200-400 nm region, with a prominent peak centered around 346 nm and a maximum absorbance of approximately 1.943. This broad spectral feature indicates the presence of various phytochemicals, including chlorophyll derivatives, flavonoids, and phenolic compounds. In contrast, the CuO nanoparticles exhibited a sharp and intense absorption band near 200 nm, which is characteristic of surface plasmon resonance associated with nanoscale metal oxides. The clear spectral shift between the extract and nanoparticle samples confirms the successful formation of CuO nanostructures. Furthermore, these observations suggest that bioactive molecules present in the algal extract play a dual role as both reducing and stabilizing agents during nanoparticle synthesis. The observed optical properties also indicate potential applications of the nanocomposite scaffolds in UV shielding and photocatalytic systems [34-37].

3.2. FTIR analysis

FTIR spectra (Figure 2) provided insight into the chemical composition of both CuO nanoparticles and the fabricated nanofibrous scaffolds. The nanoparticles exhibited a distinct absorption peak at 601 cm^{-1}, corresponding to Cu–O stretching vibrations, along with additional bands at 863 cm^{-1} and 1061 cm^{-1} attributed to metal–oxygen and C–O functional groups. A broad absorption band around 3122 cm^{-1} was associated with hydroxyl groups, likely originating from adsorbed moisture or organic compounds derived from the algal extract. The composite nanofibers showed characteristic peaks at 3284 cm^{-1} (O–H/N–H stretching), 2921 cm^{-1} (C–H stretching), and 1710 cm^{-1} (carbonyl groups), confirming the presence of starch and PVA within the scaffold. Additional peaks at 1328 cm^{-1} and 1087 cm^{-1} correspond to amine and glycosidic linkages. The simultaneous presence of Cu–O and polymer-related bands demonstrates successful nanoparticle incorporation without significant alteration of the polymeric structure [38-42].

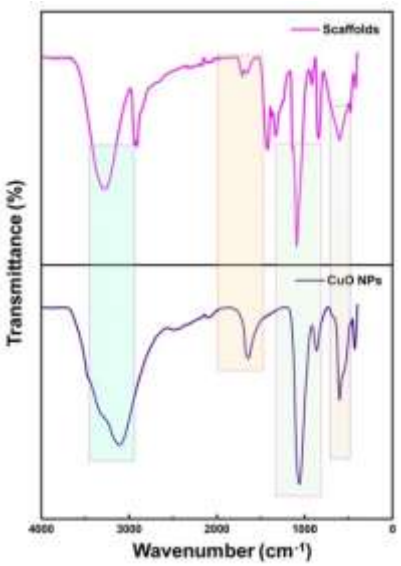

Figure 2. Infrared spectral features highlighting chemical functionalities of CuO nanostructures and their presence within the composite fiber system.

3.3. XRD analysis

The X-ray diffraction results (Figure 3) verified the crystalline nature of the prepared CuO nanoparticles as well as their successful incorporation into the nanofibrous scaffold system. The diffraction profile displayed several characteristic peaks within the 2θ interval of 5° to 90°, with notable reflections observed at 24.435°, 32.876°, and 38.504°. These peaks correspond to the standard monoclinic crystal structure of CuO, in agreement with JCPDS reference card No. 48-1548. In contrast, the nanofibrous scaffolds displayed broader and less intense diffraction peaks at 21.420°, 29.372°, and 57.572°, indicating reduced crystallinity due to the presence of the amorphous polymer matrix. The calculated crystallinity index of the composite was 17.4%. Peak broadening and slight shifts suggest effective dispersion of nanoparticles within the fibers and partial amorphization induced by polymer–nanoparticle interactions [43-46].

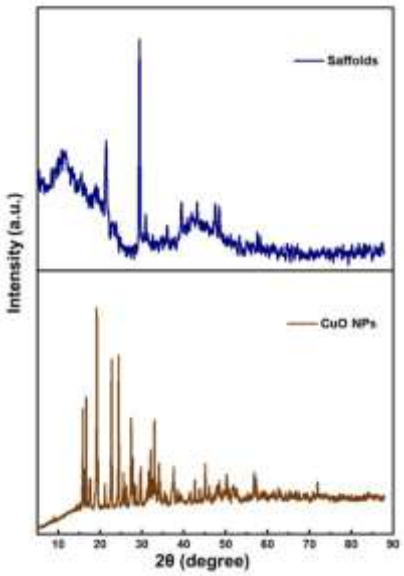

Figure 3. Diffraction profiles illustrating phase characteristics of CuO nanostructures and their distribution within the fibrous matrix.

3.4. SEM analysis

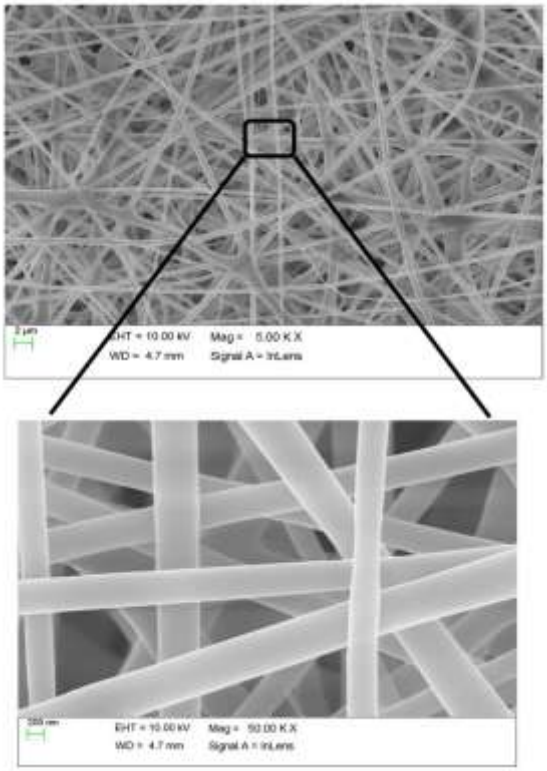

Figure 4. Electron micrographs showing fiber architecture and nanoparticle dispersion in the electrospun composite.

Morphological examination using scanning electron microscopy (Figure 4) provided detailed insight into the structural characteristics of the synthesized CuO nanoparticles and the electrospun fiber network. The nanoparticles were observed to possess mainly spherical to slightly irregular geometries, with particle sizes distributed in the range of 90-100 nm. A small degree of clustering was noted, which can be attributed to their elevated surface energy. The starch/PVA-based nanofibers exhibited a uniform and defect-free appearance, forming smooth and continuous fibers without bead formation. The average fiber diameters were found to lie between 150 and 300 nm, indicating effective control over the electrospinning process. CuO nanoparticles were uniformly distributed along the fiber surfaces, although occasional agglomerates were detected, possibly due to interparticle interactions and polymer matrix effects. The overall fibrous architecture appeared highly porous and interconnected, which is advantageous for biomedical applications such as tissue regeneration. These observations confirm successful nanoparticle synthesis and effective integration into the nanofibrous scaffold [47, 48].

3.5. Thermogravimetric analysis

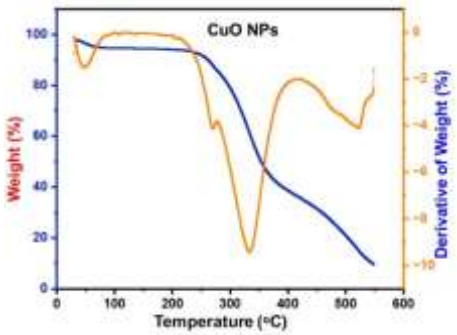

Figure 5. Thermal response profile indicating stability and degradation pattern of the nanocomposite system.

Thermal behavior of the CuO nanoparticle-incorporated scaffolds was evaluated using TGA (Figure 5). The analysis was performed by heating a 2.315 mg sample from 30°C to 550°C at a rate of 15°C/min under a nitrogen atmosphere. An initial weight loss of approximately 9.51% was observed, corresponding to the evaporation of moisture and volatile components. The primary degradation phase began around 244.81°C, with the maximum decomposition rate occurring near 332.83°C and completion at approximately 378.85°C. The total mass loss at 550°C was recorded as 41.70%. Compared to pristine polymer scaffolds, the incorporation of CuO nanoparticles delayed thermal degradation and improved overall thermal stability. This enhancement indicates that CuO nanoparticles act as reinforcing fillers within the polymer matrix [49-52].

3.6. Particle size distribution and zeta potential

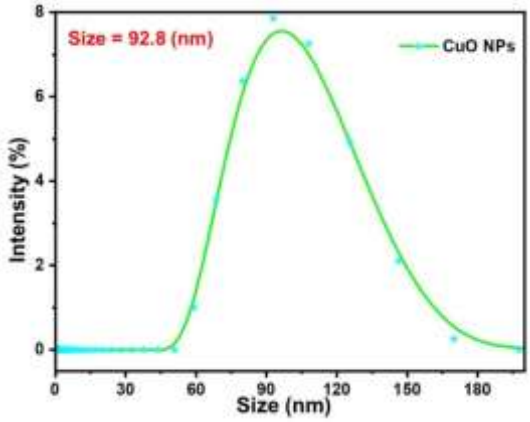

Figure 6. Hydrodynamic size distribution of synthesized CuO nanostructures obtained from light scattering measurements.

Particle size evaluation using dynamic light scattering indicated the presence of two distinct populations, reflecting a bimodal distribution pattern, with an average hydrodynamic diameter of 92.8 nm and a polydispersity index of 0.5592 (Figure 6). This distribution suggests a moderate degree of variation in particle size. The recorded scattering intensity of 3465 kcps indicates that the nanoparticle suspension maintained acceptable stability during measurement. Further analysis of surface charge through zeta potential measurements yielded a value of –5.29 mV (Figure 7), which reflects weak electrostatic repulsive forces and, consequently, limited stability of the colloidal system. This relatively low surface charge aligns with the aggregation observed in SEM images. To improve dispersion stability, surface modification or functionalization strategies may be required for future applications [53, 54].

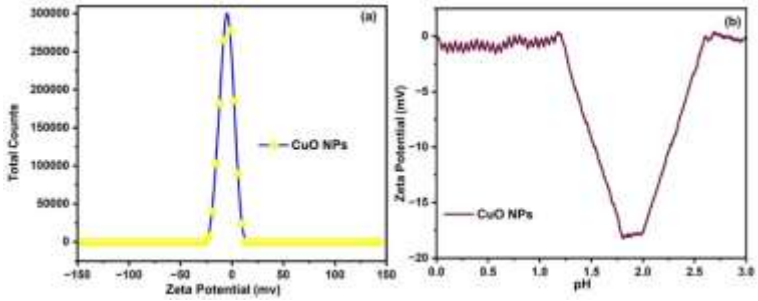

Figure 7. Surface charge characteristics reflecting dispersion behavior of CuO nanostructures.

3.7. In vitro wound healing assay

The regenerative capability of the prepared samples was examined through a scratch assay using HaCaT keratinocyte cells (Figure 8). After an incubation period of 48 hours, notable variations in cell migration and wound closure were evident across all treatment groups. At the lowest tested dose (6.25 µg/mL), the algal extract produced a closure rate of 36.03%, while treatments with CuO nanoparticles and the composite nanoscaffolds resulted in improved healing responses of 44.03% and 51.03%, respectively. With an increase in concentration to 12.5 µg/mL, the closure percentages rose to 43.03% for the extract, 50.03% for CuO nanoparticles, and 66.03% for the nanoscaffolds. A similar concentration-dependent enhancement was observed at higher doses. At 25 µg/mL, wound closure values reached 54.03%, 66.03%, and 77.03% for the extract, nanoparticles, and nanoscaffolds, respectively. Further improvement was noted at 50 µg/mL, where closure percentages increased to 64.03% for the extract, 68.03% for CuO nanoparticles, and 83.03% for the composite system. At the maximum concentration tested (100 µg/mL), the nanoscaffold formulation demonstrated almost complete wound closure (99.03%), markedly exceeding the performance of the algal extract (73.03%) and CuO nanoparticles (87.03%). These findings demonstrate that the composite nanoscaffolds markedly enhance keratinocyte migration and wound repair efficiency compared to individual components. The observed dose-dependent response highlights the importance of optimizing concentration for achieving maximum therapeutic benefit [55, 56].

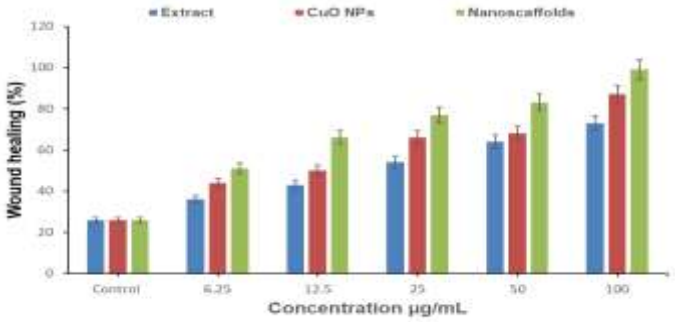

Figure 8. Evaluation of cellular migration under different treatments demonstrating wound closure efficiency.

4. DISCUSSION

This work confirms the effective generation of CuO nanoparticles through a sustainable, ultrasound-assisted green synthesis approach utilizing T. ornata extract, followed by their successful integration into electrospun starch/PVA nanofibrous scaffolds. Analysis by UV–visible spectroscopy revealed clear differences in the optical behavior of the algal extract compared to the synthesized nanoparticles, indicating the conversion of naturally derived phytochemicals into CuO nanoparticles. The broad absorption band of the crude algal extract between 200 and 400 nm, peaking at 346 nm, reflects the complex composition of marine phytochemicals such as chlorophyll derivatives, flavonoids, and phenolic compounds that contribute both as reducing and stabilizing agents during nanoparticle formation. In contrast, the sharp plasmonic absorption peak near 200 nm in the CuO NP spectrum indicates successful synthesis of nanostructured copper oxide, a signature often associated with the nanoscale dimensions and high surface energy of these materials. This spectral shift not only confirms nanoparticle formation but also suggests that these CuO nanostructures could impart functional properties such as ultraviolet (UV) light absorption, which is beneficial for wound dressings by potentially shielding wounds from harmful UV radiation [57, 58].

FTIR spectral analysis provided further confirmation of the successful integration of CuO NPs into the starch/PVA polymeric matrix. The characteristic Cu–O bond vibrations and metal-oxygen interactions in the nanoparticles were clearly identifiable alongside polymer-specific functional groups such as hydroxyl, amine, and glycosidic linkages. The presence of broad hydroxyl and carbonyl bands in the nanofiber composite confirms the retention of starch and PVA molecular structures. Importantly, the coexistence of these signals without significant shifts indicates that the incorporation process did not lead to any major chemical reactions or degradation of the polymer or the nanoparticles. This structural integrity is essential for maintaining the scaffold's biocompatibility and mechanical stability, two critical factors in wound healing applications [59-62].

XRD patterns further elucidated the crystalline nature of the synthesized CuO NPs and their distribution within the composite scaffold. The distinct monoclinic phase of CuO nanoparticles with sharp, intense diffraction peaks aligns well with standard reference data, verifying high crystallinity of the biosynthesized nanoparticles. However, the broader and less intense peaks observed in the nanofibrous scaffolds signify a reduction in crystallinity caused by the amorphous polymeric matrix, which can promote better flexibility and mechanical integrity in the final material. The partial amorphization and uniform dispersion of nanoparticles inferred from peak broadening suggest a good level of interaction at the nanoscale without phase separation, which is desirable for sustained therapeutic performance and controlled release of bioactive agents in wound healing [63-66].

The morphological features observed through SEM imaging highlight the favorable characteristics of both the nanoparticles and the composite nanofibers. The relatively uniform spherical to irregular CuO NPs, sized between 90 and 100 nm, are within an optimal size range known to enhance cellular interactions and antimicrobial effects. Although minor aggregation was noted due to high surface energy, the overall dispersion of nanoparticles within the nanofiber mat was satisfactory. The bead-free, smooth surface morphology and porous, interconnected network of starch/PVA fibers with diameters between 150 and 300 nm provide an ideal microenvironment for cell adhesion, proliferation, and nutrient transport, which are vital for effective tissue regeneration. The occasional nanoparticle clusters may be addressed in future studies by modifying electrospinning parameters or surface functionalization to achieve more homogenous distribution [67].

TGA revealed that embedding CuO NPs significantly improved the thermal stability of the starch/PVA nanofibers. The delayed onset of polymer degradation and reduced total mass loss suggest that the nanoparticles act as reinforcing agents within the polymer matrix. Enhanced thermal resistance is advantageous not only for storage and handling but also for maintaining scaffold integrity during sterilization and in situ application on wounds. This improved stability potentially prolongs the scaffold's functional lifespan during the wound healing process [68].

DLS and zeta potential measurements provided valuable insight into nanoparticle size distribution and colloidal stability, which are important for their biological behavior. The moderate polydispersity and bimodal size distribution indicate a somewhat heterogeneous nanoparticle population, which could influence cellular uptake and antimicrobial efficacy. The relatively low negative zeta potential (–5.29 mV) corresponds with the observed tendency for aggregation, which might limit nanoparticle dispersion stability in biological environments. Addressing this limitation through surface functionalization or polymer coating could enhance nanoparticle bioavailability and sustained release within the wound milieu [69].

Most importantly, the wound healing scratch assay demonstrated the pronounced biological efficacy of the starch/PVA/CuO NP nanoscaffolds. The scaffolds consistently outperformed both the crude T. ornata extract and the CuO

NPs alone across all tested concentrations, significantly accelerating HaCaT keratinocyte migration and wound closure. This synergistic effect likely arises from the combined bioactivity of the algal-derived CuO NPs and the biocompatible, porous polymeric scaffold, which together create a conducive environment for cellular proliferation and migration. The concentration-dependent enhancement in wound closure rate highlights the critical role of dosage optimization for maximizing therapeutic outcomes. Near-complete wound closure at the highest concentration underscores the nanoscaffold's potential as a next-generation wound dressing, capable of accelerating tissue repair while leveraging green synthesis and natural biomaterials [70].

Collectively, these findings validate the green synthesis approach as an effective strategy to produce functional CuO NPs and demonstrate their successful incorporation into starch/PVA electrospun scaffolds with enhanced physicochemical properties and superior wound healing potential. The integration of marine macroalgae-derived bioactives into a biocompatible polymeric matrix addresses the growing need for sustainable, effective wound care materials. Future work should focus on in vivo validation, long-term biocompatibility studies, and functionalization strategies to further improve nanoparticle dispersion and scaffold bioactivity for clinical translation.

5. CONCLUSION

This study presents an environmentally sustainable strategy for designing multifunctional nanofibrous materials by integrating marine-derived bioactive compounds with copper oxide nanostructures. The successful generation of CuO nanoparticles through a biologically mediated process and their incorporation into a starch/PVA electrospun matrix resulted in a composite system with improved structural and functional characteristics. Physicochemical analyses demonstrated that the incorporation of nanoparticles enhanced the stability and integrity of the fibrous network without compromising its chemical composition. The developed scaffold exhibited a highly porous architecture, which is advantageous for facilitating cellular interactions and supporting tissue regeneration. Biological evaluation confirmed that the composite system significantly promotes keratinocyte migration in a concentration-dependent manner, outperforming individual components. This enhanced performance can be attributed to the combined influence of the polymeric matrix and the embedded nanostructures, which together create a favorable microenvironment for wound repair. Overall, the findings highlight the potential of combining green synthesis approaches with nanofiber engineering to develop advanced wound healing materials. Future studies focusing on in vivo validation and long-term biocompatibility will further support the clinical translation of this system.

Ethical Declaration: Not applicable for this study.

Funding: Not available for this study.

Conflicts of Interest: The authors declare no conflicts of interest.

Data Availability Statement: The full dataset of physiochemical characterization associated with this work is published in Mendeley Data. **Disclosure:** The material characterization data and figures (e.g., UV, SEM, FTIR, XRD, TGA, Zeta Potential and particle sizer) presented here were generated from a common dataset and are being reused across multiple related studies on nanomaterials. All biological and environmental analyses and conclusions are original to each manuscript.

REFERENCES

1. Pei J, Kumarasamy RV, Jayaraman S, Kanniappan GV, Long Q, Palanisamy CP. Quercetin-functionalized nanomaterials: Innovative therapeutic avenues for Alzheimer's disease management. Ageing Research Reviews. 2025; 104: 102665.
2. Jayaraman S, Prasad M, Natarajan SR, Krishnamoorthy R, Alshuniaber MA, Gatasheh MK, Veeraraghavan VP, Rajagopal P, Palanisamy CP. Molecular mechanisms underlying the effects of beta-sitosterol on TGF-β1/Nrf2/SIRT1/p53-mediated signaling in the kidney of a high-fat diet and sucrose-induced type-2 diabetic rat. Chemico-Biological Interactions. 2025; 411: 111443.
3. Huang Y, Guo H, Liu Y, Jin W, Palanisamy CP, Pei J, Oz F, El-Aty AMA. Effects of Natural Polysaccharides on the Gut Microbiota Related to Human Metabolic Health. Molecular Nutrition & Food Research. 2025; e202400792.
4. Prabhakaran P, Palanisamy CP, Shanmugam A, Damodharan P, Swaminathan H, Devaraj D, Ahalliya RM, Kanniappan GV. Isolation, structural characterization, and molecular docking studies on the bioactive compound from n-Hexane extract of Emilia sonchifolia (L.) DC against the pancreatic cancer target Aurora 2 Kinase. Journal of Complementary and Integrative Medicine. 2024; 22(1): 0290.
5. Jiang H, Kumarasamy RV, Pei J, Raju K, Kanniappan GV, Palanisamy CP. Integrating engineered nanomaterials with extracellular vesicles: Advancing targeted drug delivery and biomedical applications. Frontiers in Nanotechnology. 2024; 6: 1513683.
6. Guo H, Liu Y, Wan T, Song D, Palanisamy CP, Geng J, Pei J, Özmen S, El-Aty AMA. Toward personalized cancer management: Role of precision nutrition–diet interventions. Journal of Functional Foods. 2024; 123: 106584.
7. Natarajan SR, Krishnamoorthy R, Alshuniaber MA, Al-Anazi KM, Farah MA, Rajagopal P, Palanisamy CP, Veeraraghavan VP, Jayaraman S. Identification of FOXM1 as a novel protein biomarker and therapeutic target for colorectal cancer progression: Evidence from immune infiltration and bioinformatic analyses. International Journal of Biological Macromolecules. 282 (Part 4): 137201.

8. Rajendran MS, Jayaraman S, Khan JM, Jasmine S, Prabhakaran RK, Raju MV, Chandrasekaran MK, Ahalliya RM, Kannappan P, Palanisamy CP, Kanniappan GV. Investigating the colon toxicity and carcinogenic role of monosodium glutamate compared with Dimethylhydrazine in male Wistar rats: Exploring the link to childhood colon cancer risk. Journal of King Saud University - Science. 2024; 36(11): 103507.
9. Kumarasamy RV, Natarajan PM, Umapathy VR, Roy JR, Rab SO, Saeed M, Panagal M, Mironescu M, Srinivasan GP, Palanisamy CP. Clinical Applications and Therapeutic Potentials of Advanced Nanoparticles: A Comprehensive Review on Completed Human Clinical Trials. Frontiers in Nanotechnology. 2024; 6:1479993.
10. Jin W, Pei JJ, Roy JR, Jayaraman S, Ahalliya RM, Kanniappan GV, Mironescu M, Palanisamy CP. Comprehensive review on single-cell RNA sequencing: A new frontier in Alzheimer's disease research. Ageing Research Reviews. 2024; 274: 102454.
11. Natarajan PM. Dental Bioinformnatics-Current Scope and Future perspectives. Research Journal of Pharmacy and Technology. 2022;15(5):2351-6.
12. Vidhyarekha U, Natarajan PM, Bhuminathan S, Sabarinathan J, Suba R, Vijayalakshmi P. Role of artificial intelligence in Oral Cancer. Advances in Public Health. 2024. 2024: 3664408.
13. Ganesan A, Kumar NG, Natarajan PM, Gauthaman J. Automated classification of elongated styloid processes using deep learning models-an artificial intelligence diagnostics. Frontiers in Oral Health. 2025; 5: 1424840.
14. Umapathy VR, Natarajan PM, Swamikannu B. Regenerative Strategies in Dentistry: Harnessing Stem Cells, Biomaterials and Bioactive Materials for Tissue Repair. Biomolecules. 2025; 15: 546.
15. Natarajan PM, Umapathy VR, Murali A, Swamikannu B. (2022). Computational Simulations of Identified marine-derived Natural Bioactive Compounds As Potential Inhibitors of Oral Cancer. Future Science OA. 2022; 8(3).
16. Ganesan A, Kumar NG, Natarajan PM. Solanum trilobatum leaf extract-derived silver nanoparticles downregulate the PI3K/AKT/mTOR signaling pathway and attenuate oral squamous cell carcinoma cell proliferation. Journal of Herbmed Pharmacology. 2024; 13(2): 300-307.
17. Perumal MKK, Renuka RR, Subbiah SK, Natarajan PM. Artificial intelligence-driven clinical decision support systems for early detection and precision therapy in oral cancer: a mini review. Frontiers in Oral Health. 2025; 6: 1592428.
18. Ramesh E, Ganesan A, Lakshmi KC, Natarajan PM. Artificial intelligence-based diagnosis of oral leukoplakia using deep convolutional neural networks Xception and MobileNet-v2. Frontiers in Oral Health. 2025; 6: 1414524.
19. Natarajan PM. Computational Studies on Recent Congeners of Fluoroquinolones and Nitroimidazoles for Their Use in Periodontal Therapy. Journal of Pharmacy and Bioallied Sciences. 2024; 16(5): S4731-S4740.
20. Ganesan A, Kumar NG, Natarajan PM. Anticancer activity of silver nanoparticles synthesized from aqueous leaf extract of Solanum trilobatum (Purple fruit pea eggplant) on human oral cancer cells. Journal of Herbmed Pharmacololgy. 2024; 13(2): 260-268.
21. Umapathy V, Dhanavel A, Kesavan R, Natarajan PM, Bhuminathan S, Vijayalakshmi P. Anticancer Potential of the Principal Constituent of Piper nigrum, Piperine: A Comprehensive Review. Cureus. 2024; 16(2): e54425.
22. Natarajan PM, Bhuminathan S, Rajan R, Bindu K, Loganathan K, Veerakumar R. The Crucial Role of Smoking Cessation in Preventing Oral Cancer. Journal of Pharmacy and Bioallied Sciences. 2024; 16(5): S4245-S4247.
23. Umapathy VR, Swamikannu B, Natarajan PM, Devi R, Nandini MS, Vimalarani, Vijayalakshmi P. In Silico Molecular Docking of Ocimum sanctum Phytochemicals: Targeting Key Biomarkers in Oral Cancer. Journal of Pharmacy and Bioallied Sciences. 2024; 16(5): S4792-S4799.
24. Natarajan PM, Umapathy VR. Role of transcriptomics in the study of oral cancer. Frontiers in Oral Health. 2025; 6:1524364.
25. Swamikannu B, Umapathy VR, Natarajan PM, Nandini MS, Stylin AGSQ, Vimalarani V, Rajinikanth S. Unlocking the Therapeutic Benefits of Artemisia Annua: A Comprehensive Overview of its Medicinal Properties. Journal of Pharmacy and Bioallied Sciences. 2024; 16(5): S4248-S4253.
26. Yadalam PK, Arumuganainar D, Natarajan PM, Ardila CM. Artificial intelligence-powered prediction of AIM-2 inflammasome sequences using transformers and graph attention networks in periodontal inflammation. Scientific Reports. 2025; 15: 8733.
27. Yadalam PK, Chatterjee S, Natarajan PM, Ardila CM. Comparison of light gradient boosting and logistic regression for interactomic hub genes in Porphyromonas gingivalis and Fusobacterium nucleatum-induced periodontitis with Alzheimer's disease. Frontiers in Oral Health. 2025; 6:1463458.
28. Natarajan PM, Bhuminathan S, Leela B, Bindu K, Loganathan K, Ramachandran V. Smoking and its Role in Oral Cancer. Journal of Pharmacy and Bioallied Sciences 16(5): S4242-S4244.
29. Yadalam PK, Natarajan PM, Ardila CM. Variational graph autoencoder for reconstructed transcriptomic data associated with NLRP3 mediated pyroptosis in periodontitis. Scientific Reports. 2025; 15: 1962.
30. Natarajan PM, Swamikannu B, Sivaraman NM, Stylin AGSQ. Prevention of Oral Cancer: A Comprehensive Guide. Journal of Pharmacy and Bioallied Sciences. 2024; 16(5): S4239-S4241.
31. Surendran N, Chandrasekaran G, Raju MV, Chandrasekaran MK, Ahalliya RM, Palanisamy CP, Kanniappan GV, Arcot R, Alharbi NS, Thiruvengadam M. Anti-inflammatory potential of ethanolic extract of Maranta arundinacea L.: Insights from COX-2 modulation and oxidative stress analysis. South African Journal of Botany. 2026; 195: 142-151.
32. Pei J, Senthilkumar MV, Hessini K, Subramaniyam S, Sivaramakrishnan R, Kanniappan GV, Jayaraman S, Palanisamy CP. Green fabrication of starch/PVA/CuO nanoscaffolds using marine macroalgae extract for enhanced anti-inflammatory activity. Sustainable Chemistry and Pharmacy. 2026; 51: 102397.
33. Balasubramanian V, Loganathan L, Muthuswamy K, Viswanathan TM, Raju MV, Chandrasekaran MK, Ahalliya RM, Poorasamy J, Palanisamy CP, Dominic S, Kanniappan GV. Anticancer therapeutic efficacy of PEGylated β-

galactosidase from Aspergillus terreus in DMBA-induced breast cancer: Toxicological, molecular and histopathological evaluation in Wistar rats. International Journal of Biological Macromolecules. 2026; 360: 151856.
34. Jayaraman S, Eswaran A, Rajagopal P, Palanisamy CP, Veerakumar P, Veeraraghavan VP, Sirasanagandla SR. Neuroendocrine-associated epigenetic factors in cellular senescence: mechanisms and therapeutic implications. Biogerontology. 2026; 27(2): 64.
35. Ponnusamy B, Rajagopal P, Palanisamy CP, Veeraraghavan VP, Jayaraman S. Mechanistic Exploration of the anticancer activity of Justicia adhatoda Plant Leaf Ethanolic Extract against Colon Cancer Cells: An in silico and in vitro Approach. Asian Pacific Journal of Cancer Prevention. 2026; 27(3): 1069-1080.
36. Pei J, Saran VS, Sivaramakrishnan R, Kanniappan GV, Pandurangan V, Jayaraman S, Dhayalan VK, Mironescu M, Mironescu ID, Palanisamy CP. Ultrasonic-assisted, Sargassum ilicifolium (brown marine macroalgae)-mediated biogenic synthesis of CuO nanoparticles incorporated in starch/PVA electrospun nanoscaffolds: In vitro safety and antioxidant efficacy assessment. Bioorganic Chemistry. 2026; 173: 109679.
37. Raj MAPA, Subramaniyam S, Kanniappan GV, Jayaraman S, Palanisamy CP. Sustainable fabrication of starch/PVA/CuO electrospun nanoscaffolds from Turbinaria ornata (marine macroalgae) extract: Physicochemical characterization and antidiabetic evaluation. Kuwait Journal of Science. 2026; 53(2): 100545.
38. Pei J, Ganesh NS, Subramaniyam S, Sivaramakrishnan R, Kanniappan GV, Jayaraman S, Palanisamy CP. Sustainable fabrication of starch/PVA/CuO electrospun nanoscaffolds from Padina tetrastromatica (Brown macroalgae) extract: Physicochemical characterization and antidiabetic assessment. Sustainable Chemistry One World. 2026; 9: 100195.
39. Sakthiraj A, Sivaramakrishnan R, Subramaniyam S, Kanniappan GV, Pandurangan V, Jayaraman S, Dhayalan VK, Mironescu M, Mironescu ID, Palanisamy CP. Chemical Physics Impact. Starch/PVA electrospun nanoscaffolds loaded with ultrasonic-assisted green-synthesis of CuO nanoparticles from marine macroalgae (Gracilaria corticata) extract: Cytotoxicity and antioxidant analysis. 2026; 12: 101018.
40. Raju M, Chandrasekaran MK, Loganathan L, Ahalliya RM, Mironescu M, Mironescu ID, Palanisamy CP, Kanniappan GV. Lipid remodeling and ferroptosis in phosphatidylcholine-mediated tumor–stroma crosstalk. Frontiers in Molecular Biosciences. 2026; 13: 1742305.
41. Kunamalla R, Panagal M, Palanisamy CP. Biogenic synthesis and fabrication of starch/PVA/CuO electrospun nanoscaffolds from Sargassum ilicifolium (brown marine macroalgae) extract for anticancer activity on HT-29 and MCF-7 cancer cells. Biocatalysis and Agricultural Biotechnology. 2026; 72: 103923.
42. Pei J, Govindaraj H, Sivaramakrishnan R, Kanniappan GV, Pandurangan V, Dhayalan VK, Mironescu M, Mironescu ID, Jayaraman S, Palanisamy PC. Sustainable fabrication of biopolymer-based (starch/PVA) nanoscaffolds loaded with green-synthesized CuO nanoparticles from Sargassum wightii (marine macroalgae): Cytocompatibility and antioxidant activity. Biomaterials Advances. 2026; 182: 214660.
43. Pei J, Perumal NC, Meng P, Long Q, Palanisamy CP. Extracellular vesicle-based biosensors for Alzheimer's disease: A new frontier in precision diagnostics. Ageing Research Reviews. 2026; 113: 102904.
44. Shree P, Sivaramakrishnan R, Kanniappan GV, Pandurangan V, Jayaraman S, Dhayalan VK, Mironescu M, Mironescu ID, Palanisamy CP. Antioxidant and biocompatible CuO-starch/PVA nanoscaffolds via ultrasonic green synthesis using Turbinaria conoides (brown marine macroalgae). Medicine in Drug Discovery. 2025; 28: 100238.
45. Gong J, Lin J, Guan T, Pei J, Palanisamy CP, El-AtyFrom AMA. selenium tolerance to nanoplastic antagonism: Comprehensive characterization of L. casei SNUT1 and its extracellular vesicle–nanoselenium complex. Food Bioscience. 2025; 74: 107749.
46. Poochi SP, Sundarraj R, Raju MV, Chandrasekaran MK, Ahalliya RM, Palanisamy CP, Kanniappan GV, Kondapavuluri BK, Thiruvengadam M. Harnessing Nature: Computational and Experimental Insights Into Ipomoea obscura Metabolites for Bladder Cancer Therapy. Chemistry and Biodiversity. 2025; 0: e00909.
47. Dugganaboyana GK, Kannankumar MKG, Shivaramakrishna S, Raju MV, Chandrasekaran MK, Ahalliya RM, Panneerselvam N, Palanisamy CP, Kanniappan GV. Phytochemical insights, antioxidant activity and therapeutic potential of Cassia senna against prostate cancer in Wistar albino rats. Discover Applied Sciences. 2025; 7:1206.
48. Natarajan SR, Krishnamoorthy R, Alshuniaber MA, Gatasheh MK, Rajagopal P, Veeraraghavan VP, Palanisamy CP, Jayaraman S. KDM1A Facilitates Oncogenic Potential in Colorectal Cancer Progression Through the Activation of AXIN/GSK3β/β-Catenin Signaling Pathways: Evidence From Integrated Transcriptomics and In Vitro Studies. The Journal of Gene Medicine. 2025; 27(11): e70053.
49. Guan T, Gong J, Lin J, Palanisamy CP, Jinjin Pei J, El-Aty AMA. Machine learning-driven multimodal optimization of selenium biotransformation and flavor profiling in fermented apple–Yacon functional beverages. Innovative Food Science & Emerging Technologies. 2025; 105: 104198.
50. Natarajan SR, Krishnamoorthy R, Alshuniaber MA, Alsulami TS, Gatasheh MK, Rajagopal P, Palanisamy CP, Govindan R, Veeraraghavan VP, Jayaraman S. ABCE1 facilitates tumour progression via aerobic glycolysis and inhibits cell death in human colorectal cancer cells through the p53 signalling pathway. Scientific Reports. 2025; 15: 24674.
51. Huang Y, Guo H, Liu Y, Jin W, Palanisamy CP, Pei J, Oz F, El-Aty AMA. Effects of Natural Polysaccharides on the Gut Microbiota Related to Human Metabolic Health. Molecular Nutrition & Food Research. 2025; 69:e202400792.
52. Poornima K, Meenakshi K.C, Manikandan V.R, Shankari G, Prabhu D, Rathi M.A, Palanisamy CP, Balaji R, Gopalakrishnan V.K. Exploring the anticancer potential of Jerantinine A from Tabernaemontana coronaria against prostate, breast, and ovarian cancers: A computational approach. Journal of Complementary and Integrative Medicine, 2025 22(2): 363–372.

53. Palanisamy CP, Poompradub S, Sansanaphongpricha K, Jayaraman S, Subramani K. Faridah Sonsudin gGreen synthesis of Nigella sativa-mediated silver nanoparticles for enhanced antibacterial activity and wound healing: Mechanistic insights and biomedical applications. Environmental Nanotechnology, Monitoring & Management. 2025; 24: 101085.
54. Surendran N, Raju MV, Chandrasekaran MK, Ahalliya RM, Palanisamy CP, Chandrasekaran G, Kanniappan GV. Physicochemical characterization of starch from Maranta arundinacea L.(arrowroot) rhizomes and its inhibition of COX-2: In vivo validation. Bioactive Carbohydrates and Dietary Fibre. 2025; 33: 100465.
55. Kannappan P, Chandrasekaran MK, Raju MV, Gopalakrishnan S, Dhamodharan P, Ahalliya RM, Palanisamy CP, Raju B, Kanniappan GV. Exploring the anticancer potential of Jerantinine A from Tabernaemontana coronaria against prostate, breast, and ovarian cancers: a computational approach. Journal of Complementary and Integrative Medicine. 2025; 22(02): 363-372.
56. Pei J, Palanisamy CP, Jayaraman S, Natarajan PM, Umapathy VR, Roy JR, Panagal M, Jayaraman S. Curcumin-loaded polymeric nanomaterials as a novel therapeutic strategy for Alzheimer's disease: A comprehensive review. Ageing Research Reviews. 2024; 99: 102393.
57. Pei J, Palanisamy CP, Jayaraman S, Natarajan PM, Umapathy VR, Roy JR, Thalamati D, Ahalliya RM, Kanniappan GV*, Mironescu M. A comprehensive review on starch-based Sustainable Edible Films Loaded with Bioactive Components for Food Packaging. International Journal of Biological macromolecules. 2024; 274 (Part-1): 133332.
58. Palanisamy CP, poompradub S, Sansanaphongpricha K, Subramani K, Sonsudin F. Increased expression levels of PDGF and VEGF magnify the wound healing potential facilitated by biogenic synthesis of silver nanoparticles. Nano-Structures & Nano-Objects. 2024; 39: 101236.
59. Pei J, Palanisamy CP, Jayaraman S, Natarajan PM, Umapathy VR, Roy JR, Thalamati D, Ahalliya RM, Kanniappan GV, Mironescu M. Proteomics Profiling of Extracellular Vesicle for Identification of Potential Biomarkers in Alzheimer's Disease: A Comprehensive Review. Ageing Research Reviews. 2024; 99: 102359.
60. Xi J, Wang T, Xian P, Liu X, Du M, Yang H, Palanisamy CP, Lin W, Long Q. Proteomic insights uncover enhanced neurotherapeutic potential in conditioned mesenchymal stem cell-derived extracellular vesicles. Extracellular Vesicle. 2024; 3: 100037.
61. Pei J, Natarajan PM, Umapathy VR, Swamikannu B, Sivaraman NM, Krishnasamy L, Palanisamy CP. Advancements in the synthesis and functionalization of zinc oxide-based nanomaterials for enhanced oral cancer therapy. Molecules. 2024; 29(11): 2706.
62. Gatasheh MK, Natarajan SR, Krishnamoorthy R, Alsulami TS, Rajagopal P, Palanisamy CP, Veeraraghavan VP, Jayaraman S. Molecular analysis to identify novel potential biomarkers as drug targets in colorectal cancer therapy: an integrated bioinformatics analysis. Molecular and Cellular Oncology. 2024; 11(1): 2326699.
63. Pei J, Yan Y, Jayaraman S, Rajagopal P, Natarajan PM, Umapathy VR, Gopathy S, Roy JR, Sadagopan CS, Thalamati D, Palanisamy CP, Mironescu M. A review on advancements in the application of starch-based nanomaterials in biomedicine: Precision drug delivery and cancer therapy. International Journal of Biological Macromolecules. 2024; 130746.
64. Pei JJ, Yan Y, Palanisamy CP, Jayaraman S, Natarajan PM, Umapathy VR, Gopathy S, Roy JR, Sadagopan JC, Thalamati D, Mironescu M. Materials-based drug delivery approaches: Recent advances and future perspectives. Green Processing and Synthesis. 2024; 13: 20230094.
65. Panneerselvam S, Viswaja K, Deepa E, Prathiba S, Rebecca FS, Nivedha RP, Rajagopal P, Veeraraghavan VP, Sridevi G, Palanisamy CP, Jayaraman S. Hypoglycemic Potential of Acalypha indica in Streptozotocin-Induced Type 2 Diabetic Rats. International Journal of Drug Delivery Technology. 2026; 16(26s):1038-1047.
66. Panneerselvam S, Viswaja K, Prathiba S, Rebecca FS, Nivedha RP, Rajagopal P, Fathima SJH, Veeraraghavan VP, Sridevi G, Palanisamy CP, Jayaraman S. Acalypha Indica Attenuates Insulin Resistance in STZ-Induced Type 2 Diabetic Male Rats: Mechanistic Study. International Journal of Drug Delivery Technology. 2026; 16(26s):1027-1037.
67. Manju NE, Natarajan A, Rebecca FS, Nivedha RP, Hemalatha R, Rajagopal P, Murali R, Veeraraghavan VP, Sridevi G, Palanisamy CP, Jayaraman S. Effect of Seendhil polyherbal formulation in attenuating type-2 diabetes in STZ-induced experimental rats. International Journal of Drug Delivery Technology. 2026; 16(26s):981-989.
68. Manju NE, Natarajan A, Rebecca FS, Nivedha RP, Hemalatha R, Rajagopal P, Murali R, Veeraraghavan VP, Sridevi G, Palanisamy CP, Jayaraman S. Molecular mechanism to identify the effects of Seendhil polyherbal preparation on IRS-1/AKT/GLUT4/NRF2-KEAP-1 mediated signaling in SFZ-induced type-2 diabetic adult male rats. International Journal of Drug Delivery Technology. 2026;16(26s):972-980.
69. Palanisamy CP, Poompradub S, Sansanaphongpricha K, Jayaraman S, Subramani K, Sonsudin F. Biosynthesis of silver nanoparticles (AgNPs) using ethanolic extract of Nigella sativa (L.) seeds promotes wound healing via PDGF and VEGF signalling pathways activation. Biocatalysis and Agricultural Biotechnology. 2023; 54: 102970.
70. Palanisamy CP, Pei JJ, Phaniendra A, Venkata AAN, Jayaraman S, Veeraragahavan VP, Sridevi G, Roy JR, Janaki CS, Thalamati D, Mironescu M, Luo Q, Chai Y, Long Q. New Strategy of Neurodegenerative Disease Treatment with Extracellular Vesicles (EVs) Derived from Mesenchymal Stem Cells (MSCs). Theranostics. 2023; 13(12):4138-4165.